

Conductance Quantization in Graphene Nanoribbons

Yu-Ming Lin,* Vasili Perebeinos, Zhihong Chen, and Phaedon Avouris
IBM T. J. Watson Research Center, Yorktown Heights, NY 10598, USA

We report the experimental observation of conductance quantization in graphene nanoribbons, where 1D transport subbands are formed due to the lateral quantum confinement. We show that this quantization in graphene nanoribbons can be observed at temperatures as high as 80 K and channel lengths as long as 1.7 μm . The observed quantization is in agreement with that predicted by theoretical calculations.

The isolation of graphene [1], a single sheet of graphite, has incited numerous studies because of fundamental physics interests[2, 3] and promising applications for carbon-based electronics[4]. As a truly two-dimensional system and a zero-gap semiconductor where the electrons and holes behave as massless fermions, graphene possesses distinctly different transport properties from that of conventional 2D and 3D electronic materials. However, in order to utilize their remarkable electrical characteristics in certain applications, it would be highly desirable to produce a band gap in graphene, and therefore, intense efforts are being made to explore the properties of low-dimensional (1D and 0D) graphene nanostructures[5, 6, 7, 8].

By patterning graphene into a narrow ribbon structure, the carriers are laterally confined to form a quasi-one-dimensional (1D) system, similar to the case of carbon nanotubes. Due to the linear dispersion relation $E = v_f \hbar k$ and high Fermi velocity ($v_f \sim 10^6 \text{m/s}$) in graphene, the quantization energy of graphene nanoribbons (GNRs) can be substantially larger than that of conventional semiconducting materials of the same dimension and parabolic dispersion. The formation of 1D subbands in GNRs is expected to yield an energy gap for certain ribbon widths and crystallographic directions [9]. In terms of transport, this quantum confinement can also lead to quantized conductance, which is one of the most important transport characteristics of mesoscopic physics.

Recently, experimental studies on GNRs have revealed a thermally-activated conductivity [5, 6], suggesting the presence of a size-dependent energy gap. However, there remains some controversy in understanding the transport behavior in realistic GNR devices, where the imperfect and unknown edge configurations may lead to Coulomb-blockade type transport at low temperatures [8]. Furthermore, an energy gap could also be induced by substrate interactions [10]. Despite numerous theoretical predictions on GNRs [11, 12, 13], conductance quantization has yet to be reported experimentally.

In this Letter, we present electrical transport measurements for GNR devices with lateral widths of 30 nm, and report conductance plateau features in GNRs at temperatures as high as 80 K. By modulating the Fermi energy by a back gate, we observe conductance quantiza-

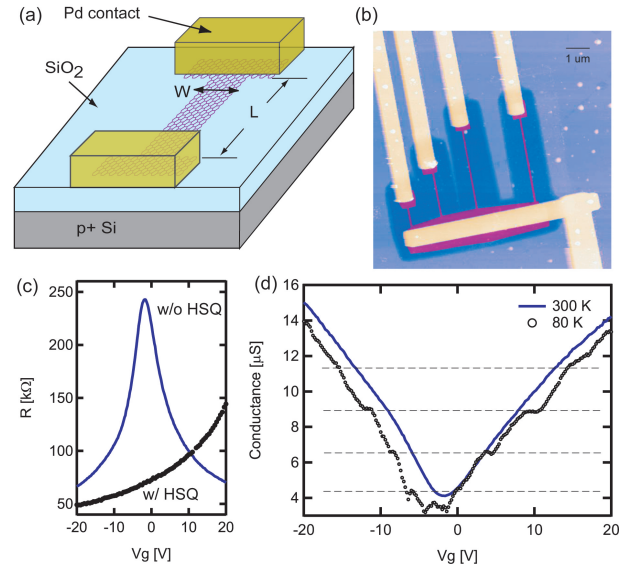


FIG. 1: (a) Schematics of the GNR device, where the graphene is contacted by two Pd metal leads, and the p -doped Si substrate acts as the gate electrode. (b) AFM image of GNR devices with different channel lengths. (c) Resistance of a GNR device measured as a function of gate voltage before and after the HSQ layer is removed, showing the impact of HSQ on electrical behaviors. Both measurements were performed in vacuum after annealing at 135 $^\circ\text{C}$. (d) Conductance of a GNR device ($W = 30 \text{nm}$ and $L = 850 \text{nm}$) measured as a function of gate voltage at 300 K and 80 K. The bias voltage is 10 mV.

tion plateaus for electron and holes in the same device, both possessing comparable transmission probability for each 1D conduction mode. Our results provide the direct experimental evidence of quantum size confinement effects and the formation of subbands for 1D graphene nanostructures.

The GNR devices in our study, schematically shown in Fig. 1(a), were fabricated from mechanically-exfoliated graphene sheets on a p -doped Si substrate covered with 300-nm thick SiO_2 . Raman spectroscopy and atomic force microscope (AFM) measurements were employed to identify single-layer graphene. For the details of the device fabrication, we refer to Ref. [6, 14]. The source and drain contacts are made of Pd, and the Si substrate acts as the back gate. Narrow ribbons of graphene are formed by oxygen plasma RIE etching using a patterned

HSQ (hydrogen silsesquioxane) layer as the protective mask. Fig. 1(b) shows the AFM image of an array of 30-nm-wide GNRs after this HSQ layer is removed in hydrofluoric acid (HF) solution. We found that electrical properties of the GNRs are strongly affected by this HSQ layer, which needs to be removed in order to reveal their intrinsic transport properties and, more importantly, the conductance quantization behaviors at low temperatures, as discussed below. Fig. 1(c) shows the resistance as a function of gate voltage V_g of a GNR device before and after the HSQ layer is removed. We note that the presence of HSQ leads to a significant positive shift of the Dirac point voltage and a reduction of carrier mobility in graphene. In contrast, after removing the HSQ layer, the GNR exhibits ambipolar behavior with the resistance maximum associated with the Dirac point occurring at $V_g \simeq 0$ V, indicating a negligible unintentional doping in the final device.

Transport measurements of GNRs were performed in vacuum ($\sim 10^{-7}$ torr), and the devices studied all possess a Dirac voltage near $V_g \sim 0$ V after annealing at 135°C . Fig. 1(d) shows the conductance G of a GNR device ($L = 850$ nm and $W = 30$ nm) measured as a function of gate voltage V_g at a dc bias of 10 mV. At room temperature, the conductance curve $G(V_g)$ in Fig. 1(d) resembles that of bulk graphene [2], showing the characteristic "V" shape that reflects symmetric hole and electron transports at negative and positive gate voltages, respectively. While the overall conductance curve $G(V_g)$ of the GNR displays little variation as temperature decreases, several plateau features start to appear in the measured $G(V_g)$ curve and become apparent for $T < 100$ K (see Fig. 1(d)). The slight asymmetry in the slope of the n and p branches is likely associated with the gate oxide hysteresis. Nevertheless, we note that these conductance plateaus are observed in both electron and hole branches with nearly the same conductance values and an equal spacing (see dashed line in Fig. 1(d)).

Conductance plateau features similar to those found in Fig. 1(d) are also observed in other 30-nm-wide GNR devices for channel lengths L up to $1.7 \mu\text{m}$. Figs. 2(a) and (b) show the $G(V_g)$ measured for two GNRs with $L = 900$ nm and $1.7 \mu\text{m}$, respectively. At low temperatures, both GNRs exhibit equally-spaced conductance steps as V_g varies. From Fig. 1(d) and Fig. 2, while the spacing ΔG between conductance plateaus depends on the channel length, where ΔG decreases with increasing L , the number of plateaus is roughly constant in the same gate voltage span (~ 20 V) for these GNRs of the same width. It is also important to note that these conductance plateau structures are highly reproducible under different thermal cycles, and they generally become more well-defined as T decreases, in particular for longer channel devices. However, as the temperature further decreases below 10 K, the $G(V_g)$ traces of these GNRs are usually overwhelmed by a pronounced fluctuation back-

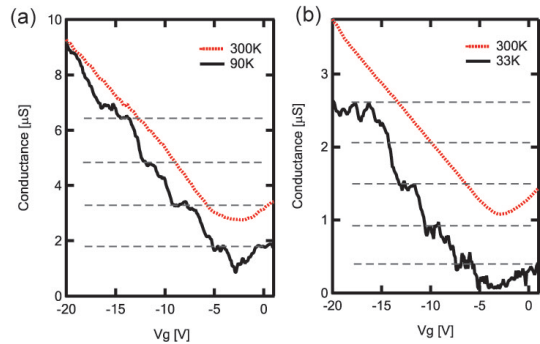


FIG. 2: Conductance measured as a function of gate voltage for 30-nm-wide GNR devices with different channel lengths. The GNR channel lengths are 900 nm and $1.7 \mu\text{m}$ for (a) and (b), respectively. At low temperatures, both devices show equally-spaced conductance plateaus with $\Delta G \simeq 1.7 \mu\text{S}$ and $0.6 \mu\text{S}$ for (a) and (b), respectively. The bias voltage is kept at 10 mV.

ground as a function of gate voltage. Unlike the plateau structures, the low- T background fluctuations are not traceable in different thermal cycles, indicating that the low- T background fluctuations may be due to the universal conductance fluctuation (UCF) phenomena [6].

Based on these experimental findings, we attribute the conductance plateaus observed in GNRs to the formation of 1D conduction modes in nanoribbons. There have been numerous theoretical studies on the GNR electronic structure and its dependence on the ribbon width and the cutting angle using π -orbital tight-binding models [11, 12] and the first principle calculations [13, 15]. To a first order approximation, the band structure of GNRs can be described by zone folding the graphene band structure. In a graphene nanoribbon of width W , the wave vector perpendicular to the transport direction has a quantization requirement $k_{\perp}W = \pi m$, giving rise to various 1D subbands, each with the dispersion relation given by

$$E_m(k_{\parallel}) = \pm \hbar v_f \sqrt{k_{\parallel}^2 + (m + \alpha)^2 \pi^2 / W^2}, \quad (1)$$

where $m = 0, \pm 1, \pm 2, \dots$ is an integer for the subband index and k_{\perp} and k_{\parallel} are the wave-vector perpendicular and parallel to the transport direction, respectively. Here $0 \leq |\alpha| < 0.5$ depends on the crystallographic orientation of the GNR, and yields a bandgap $\Delta_{GNR} = 2\Delta E|\alpha|$, where $\Delta E = \hbar v_f \pi / W$ is the energy separation between the 1D subbands. We note that in GNRs, the wavefunction has to vanish at the ribbon edges, in contrast to the periodic boundary condition in the case of carbon nanotubes (CNTs). This leads to a different quantization requirement in CNTs, namely $k_{\perp}W_{\text{CNT}} = 2\pi m$, and as a result twice as large energy separation in CNTs for the same circumference length W . In addition, the 1D subbands of GNRs are singly degenerate as opposed to those of CNTs [16], where the orbital degeneracy associated with the K-K' bands is lifted with the splitting

determined by the GNR chirality.

For a more realistic model of the GNR band structure, we adopt the tight-binding method with the next-neighbor hopping $t_C = 2.7\text{eV}$. The Fermi velocity is related to the hopping integral t according to $v_f = 3at_C/2\hbar \simeq 10^6\text{ m/s}$, where $a \approx 0.246\text{ nm}$ is a lattice constant of graphene. At the ribbon edge, we assume enhanced hopping between the neighboring C atoms by 12% to account for the C-C bond length contraction [17]. We find that in armchair GNRs (unrolled zigzag CNTs), $\alpha \approx 0.27, 0.4,$ and 0.066 in the families $N = 3p, N = 3p + 1, N = 3p + 2$ respectively, where p is an integer and N is the number of dimer lines across the ribbon width. As a result, the K-K' orbital splitting in families $N = 3p + 1$ and $N = 3p + 2$ is about $0.2\Delta E$ and $0.13\Delta E$, respectively. On the other hand, for the $N = 3p$ family, the subband energies are separated by $0.46\Delta E$ (or $0.54\Delta E$), such that the resulting subbands are roughly equally spaced with half the quantization energy ΔE .

Using the Landauer approach, the device conductance at a finite temperature can be expressed by

$$G = \frac{2e^2}{h} \sum_i \int T_i(E) \left(-\frac{\partial f_0}{\partial E} \right) dE, \quad (2)$$

where $T_i(E)$ is the transmission probability of carriers in each subband at energy E , and the factor 2 comes from the spin degeneracy. At zero temperature, Eq. (2) can be reduced to $G = 2e^2/h \sum_i t_i$ where $t_i = T_i(E_f)$ and the summation includes all the 1D modes below the Fermi energy. In our simulation, we assume an energy-independent transmission probability t for all subbands.

Now we compare simulations of the GNRs with the experimental results. For a 30-nm-wide GNR as shown in Fig. 1, we estimate the quantization energy ΔE to be 60 meV. From simulations based on Eq. (2), we find that an energy spacing of at least $6kT$ is required in order to observe conductance quantization features at a given temperature T . Since the conductance steps are clearly visible in Fig. 1 at 80 K, corresponding to a minimum energy separation of 40 meV, the energy splitting at the K-K' bands must be smaller than 20 meV. These facts can be accounted for, within the tight-binding model, by adopting a $(3p+1)$ family armchair ribbon to model the electronic structure of the GNR in Fig. 1. Fig. 3(a) shows the calculated density of states of an armchair GNR with $N = 253$, corresponding to $W=31\text{ nm}$. The quantization energy in this ribbon is $\Delta E \approx 58\text{ meV}$ and the separation between the nearly degenerate pairs of bands is about $\Delta E' = 0.8\Delta E \approx 46\text{ meV}$. Indeed, we find an excellent agreement between the measurement and the simulation at 80 K as shown in Fig. 3(b). In Fig. 3(b), the step height is $4e^2/h$ because the steps associated with individual occupation of nearly degenerate bands, which are separated by only 11 meV, cannot be resolved at this temperature.

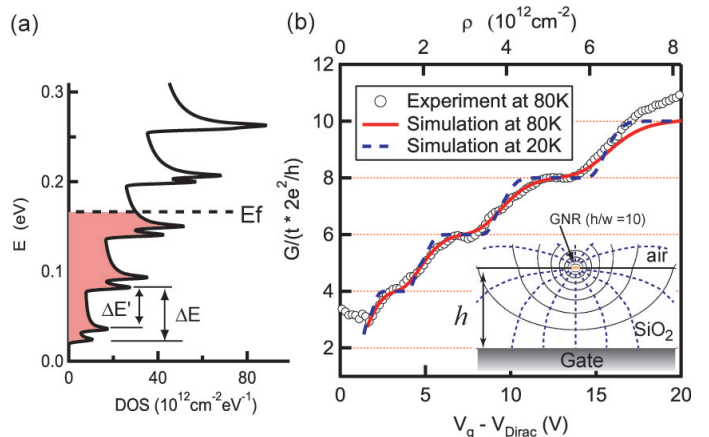


FIG. 3: (a) The density of states of a graphene nanoribbon. (b) Calculated normalized conductance $G/(2te^2/h)$ as a function of carrier density for graphene nanoribbon devices of $W = 31\text{ nm}$, using armchair GNR with $N = 253$. The inset illustrates schematically the field lines and the equipotential surfaces of the GNR, demonstrating a significant discrepancy from the case of a parallel-plate capacitor.

In order to further resolve these nearly degenerate subbands, the measurements should be performed below 10 K, the regime where universal conductance fluctuation dominate the transport properties. From Fig. 3(b), we calculate the transmission probability t of this GNR to be 0.016. We note that while the transmission probability may be a function of the length, energy and the contact to the sample, the experimental results Fig. 3(b) can be well-described by a constant t at low energies. On the other hand, the discrepancy between the simulated and measured conductance of the fourth plateau around $V_g \geq 17\text{ V}$ may be associated with the enhanced transmission probability at high energies.

The carrier density in the GNR is related to the gate voltage as $\rho = C_g(V_g - V_{\text{Dirac}})$, where C_g is a gate capacitance and V_{Dirac} is a gate voltage corresponding to the Dirac point. As shown by Fig. 3(b), we observe four conductance plateaus over a V_g span of 20 V, corresponding to a shift of the Fermi level by $E_f \approx 260\text{ meV}$ and a change in carrier density of $8.4 \times 10^{12}\text{ cm}^{-2}$. This is comparable to the carrier density in 2D graphene at the same Fermi energy E_f given by $\rho_{2D} = E_f^2/\pi v_f^2$. The dependence of ρ on V_g leads to an effective gate capacitance of $C_{\text{GNR}} = 4.2 \times 10^{11}\text{ cm}^{-2}\text{V}^{-1}$, which is significantly larger than the value expected for 2D graphene, given by $C_{2D} \simeq 7.2 \times 10^{10}\text{ cm}^{-2}\text{V}^{-1}$ for the gate dielectric of SiO_2 with thickness $h = 300\text{ nm}$. This difference is due to the fact that when the aspect ratio of the GNR width to the oxide thickness (w/h) becomes much smaller than one, the field lines between the GNR and the gate deviates from that of a parallel-plate capacitor (see inset of Fig. 3(b)), resulting in an increasing C_{GNR}/C_{2D} ratio as

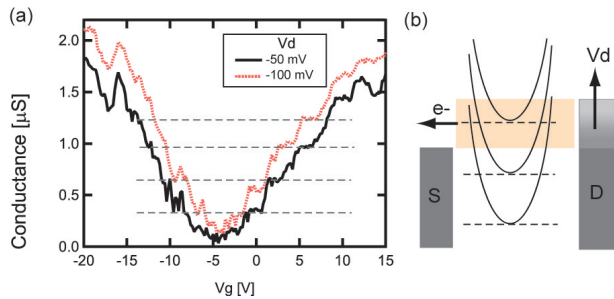


FIG. 4: (a) Conductance of a GNR device measured as a function of gate voltage at $T=15$ K for two drain biases, 50 mV and 100 mV. The GNR device has a channel length and width of $1.7 \mu\text{m}$ and 30 nm, respectively. (b) Schematic energy band diagram of a GNR with a drain bias voltage applied. The conductance is determined by the number of 1D subbands accessible in the bias window. For a given gate voltage, the number of 1D modes contributing to the transport can be increased at a sufficiently large drain bias.

(w/h) decreases. We have numerically calculated the capacitance of the GNR of infinite length L in the back gate configuration where the SiO_2 dielectrics and the vacuum below and above the ribbon are explicitly considered. For $h/w=300/30$, we find $C_{\text{GNR}}/C_0 \simeq 10$ [18], which is within a factor of 2 of the estimated values based on experiments[19].

We also note that, since the device conductance at room temperature is comparable to its low temperature value, the scattering mechanism is not temperature sensitive in these GNRs, and therefore, the dominate scattering process is mostly due to the impurity scattering within the channel or the edge disorders. This results in a transmission probability that decreases with the increasing channel length. It also implies that these 1D transport channels are not ideally ballistic. The fact that similar conductance quantization is observed for both electrons and holes reflects the symmetry in the electron and hole band structures as well as in their transmission probability.

In addition to the Fermi level modulation by the gate control, the number of 1D conduction modes that contribute to the transport in GNRs also depends on the bias voltage between the source and drain contacts, yielding a V_d -dependent device conductance in GNRs.[11] Fig. 4(a) shows measured conductance of a GNR device ($W = 30$ nm and $L = 1.7 \mu\text{m}$) as a function of V_g for two bias voltages V_d of 50 mV and 100 mV at 15 K, both exhibiting conductance plateaus with the same quantization spacing ΔG as V_g varies. However, in Fig. 4(a), it is noted that the conductance curve $G(V_g)$ at $V_d = 100$ mV is always higher than that of $V_d = 50$ mV by roughly one unit of quantized conductance ΔG for all gate voltages. In comparison, at $V_d = 10$ mV, this GNR possesses a nearly identical $G(V_g)$ curve to that at $V_d = 50$ mV. This dependence of conductance on the drain bias can be un-

derstood through the schematic shown in Fig. 4(b). As the source-drain bias windows becomes larger than the energy spacing of the 1D subbands, which is ~ 67 meV for a 30-nm-wide GNR, the number of 1D conduction modes is increased by one regardless of the gate voltage, resulting in a higher conductance level by ΔG .

In conclusion, we have fabricated graphene nanoribbon devices and reported the first experimental observation of conductance quantization phenomena in GNRs at temperatures as high as 80 K and channel lengths up to $1.7 \mu\text{m}$. We have performed temperature and bias dependence studies, and shown that the energy spacing between 1D subbands of 30-nm-wide GNRs is around 50 meV. The experimental results are in excellent agreements with theoretical calculations within the tight-binding approximation. The experimental findings here provide an important step towards developing graphene-based quantum devices.

The authors thank Bruce Ek for expert technical assistance.

* Electronic address: yming@us.ibm.com

- [1] K. S. Novoselov, A. K. Geim, S. V. Morozov, D. Jiang, M. I. Katsnelson, I. V. Grigorieva, S. V. Dubonos, and A. A. Firov, *Nature* **438**, 197 (2005).
- [2] A. K. Geim and K. S. Novoselov, *Nature Mater.* **6**, 183 (2007).
- [3] A. H. Castro Neto, F. Guinea, N. M. R. Peres, K. S. Novoselov, and A. K. Geim, arXiv:0709.1163 (2007).
- [4] P. Avouris, Z. Chen, and V. Perebeinos, *Nature Nanotechnology* **2**, 605 (2007).
- [5] M. Y. Han, B. Ozyilmaz, Y. Zhang, and P. Kim, *Phys. Rev. Lett.* **98**, 206805 (2007).
- [6] Z. Chen, Y.-M. Lin, M. J. Rooks, and P. Avouris, *Physica E* **40**, 228 (2007).
- [7] C. Stampfer, J. Guttinger, F. Molitor, D. Graf, T. Ihn, and K. Ensslin, *Appl. Phys. Lett.* **92**, 012102 (2008).
- [8] F. Sols, F. Guinea, and A. H. C. Neto, *Phys. Rev. Lett.* **99**, 166803 (2007).
- [9] K. Nakada, M. Fujita, G. Dresselhaus, and M. S. Dresselhaus, *Phys. Rev. B* **54**, 17954 (1996).
- [10] S. Zhou, G.-H. Gweon, A. Fedorov, P. First, W. D. Heer, D.-H. Lee, F. Guinea, A. Castro Neto, and A. Lanzara, *Nature Mater.* **6**, 770 (2007).
- [11] N. M. R. Peres, A. H. C. Neto, and F. Guinea, *Phys. Rev. B* **73**, 195411 (2006).
- [12] D. Dunlycke, D. A. Areshkin, and C. T. White, *Appl. Phys. Lett.* **90**, 142104 (2007).
- [13] J. Fernandez-Rossier, J. J. Palacios, and L. Brey, *Phys. Rev. B* **75**, 205441 (2007).
- [14] Y.-M. Lin and P. Avouris, *Nano Lett.* p. ASAP (2008).
- [15] L. Yang, C.-H. Park, Y.-W. Son, M. L. Cohen, and S. G. Louie, *Phys. Rev. Lett.* **99**, 186801 (2007).
- [16] C. T. White, J. Li, D. Gunlycke, , and J. W. Mintmire, *Nano Lett.* **7**, 825 (2007).
- [17] Y.-W. Son, M. L. Cohen, , and S. G. Louie, *Phys. Rev. Lett.* **97**, 216803 (2006).
- [18] The gate capacitance of GNRs can also be approximated

by the following semi-analytical approach. Assuming a homogenous dielectric medium ϵ below and above the GNR, the capacitance due to the back gate can be expressed by $\frac{C_Q}{C} = \frac{2}{\pi} \arctan \frac{W}{4h} + \frac{W}{4h\pi} \ln \left(1 + \frac{16h^2}{W^2} \right)$, where $C_0 = \epsilon\epsilon/h$. The solution assumes a constant charge density on the GNR. The gate capacitance of the device is

then approximated by $C_{\text{GNR}} \simeq (C_0^{\text{air}} + C_0^{\text{SiO}_2})/2$, yielding an enhancement factor of 9.

[19] The actual gate capacitance of the GNR is expected to be smaller than the numerical simulations because of (i) the non-ideal dielectrics used and (ii) the screening from source and drain electrodes.